Correlations between Li-Ion Concentration, Solvation Structure, and Equilibrium Potential of Li–Naphthalenide Solution for Li Alloying of Si Negative Electrode of Next-Generation Batteries

Fumisato Ozawa,[1,*] Yusuke Himata,[1] Hikaru Enomoto,[1] Shota Azuma,[1]

Akihiro Nomura,[2] and Morihiro Saito[1,]**

[1] *Department of Science and Technology, Seikei University,*

3-3-1 Kichijoji-kitamachi, Musashino, Tokyo 180-8633, Japan

[2] *Research Center for Energy and Environmental Materials,*

National Institute for Materials Science, Tsukuba, Ibaraki 350-0044, Japan

[*]E-mail: fumisato-ozawa@st.seikei.ac.jp

[**]E-mail: mosaito@st.seikei.ac.jp

Telephone number: +81-422-37-3750

Abstract

Lithium (Li) is a beneficial metal for use in the negative electrode (NE) of next-generation batteries, such as Li–S and Li–O_2 batteries, because it can greatly increase the energy density compared with those of conventional Li-ion batteries. However, Li dendrite growth is a serious problem for the practical use of the Li NE because of cell short circuits. Using a Si NE can solve this problem, but the Si NE does not include a source of Li as the carrier ion. Therefore, Li pre-doping of the Si NE will become important for next-generation batteries. In this study, we prepared Li–naphthalenide (Li–NTL) solutions using Li foil, naphthalene, and 2-methyltetrahydrofuran as the solvent and investigated the effect of the Li concentration on the Li alloying behavior. In particular, the changes in the solvation structure and equilibrium potential of the Li–NTL solution and the resulting Li alloying depth of the Si NE were evaluated to clarify the Li alloying mechanism of Li–NTL solution. Higher Li concentration in the Li–NTL solution generated a larger amount of the $[NTL]^{2-}$ dianion than the $[NTL]^{\bullet-}$ monoanion radical, and the solution exhibited a lower equilibrium potential. This led to deeper Li alloying of the Si NE, corresponding to a high pre-doping capacity of ~3000 mAh g^{-1} for 24 h treatment. Furthermore, the initial irreversible capacity of a Li half-cell constructed using the Li pre-doped Si NE was reduced compared with that of a Li half-cell constructed

using the pristine Si NE, and the Li half-cell maintained a high capacity. The Li concentration was found to be important in controlling the amount of dianions in the Li–NTL solution, and it determines the depth of Li alloying in the Si NE.

Keywords

Si anode, Li pre-doping, Prelithiation, Li–naphthalenide, Radical anions, Next-generation batteries

Introduction

To achieve the goal of carbon neutrality by 2050, progress in battery technology is important for energy infrastructure. This will promote the fabrication of electric vehicles and increase the capabilities of solar and wind renewable energy generation. In recent years, advanced Lithium ion (Li-ion) batteries and next-generation batteries, such as Li–S[1–4] and Li–O_2,[5–8] have been studied in parallel to increase the energy density beyond that of conventional lithium-ion batteries. In general, Li is used as the negative electrode (NE) metal of Li-ion batteries because of its high theoretical capacity (3860 mAh g^{-1}). However, Li dendrite growth of the Li metal NE occurs during charge–discharge cycling, leading to short circuits of the cells. Si is a good alternative to Li for the NE because of its

comparable capacity with Li metal (theoretical capacity of 3580 mAh g^{-1}) and rich available resources.[9] However, the next-generation batteries described above generally do not contain Li^+ ions as charge carriers in the positive electrode. Therefore, Li pre-doping of the Si NE is important for the practical application of such batteries.

Various Li pre-doping methods for the Si NE have been reported, such as directly contacting the electrode with Li metal/powder,[10,11] controllable electrochemical reactions,[12–16] and chemical reactions with reductive Li–arene complex solutions.[17–24] Among these methods, methods using chemical reactions have attracted attention because the active material can be uniformly lithiated by immersion in Li–arene complex solutions. Abe et al.[25] reported that the formation of a Li–graphite intercalation compound depends on the solvent used to prepare the Li–naphthalenide (Li–NTL) solution. Inaba et al.[26] reported that the Si electrode pre-doped with 0.5 M Li–NTL in tetrahydrofuran (THF) has a capacity of ~1300 mAh g^{-1}. It has been reported that the amount of Li pre-doping depends on the type of solute and solvent of the Li pre-doping solution. Other acene-based molecules, such as biphenyl, anthracene, and *p*-terphenyl, have been investigated as the solute of the Li–arene complex solution.[27–32] It has been reported that Li–NTL solution prepared using 2-methyl tetrahydrofuran (MeTHF) as the solvent shows a low solution equilibrium potential and achieves high Li pre-doping depth of graphite and Si

electrodes.[33–35] Specifically, we previously reported that the contact ion pair (CIP)/solvent-separated ion pair (SSIP) ratio of Li–NTL solution in MeTHF is higher than that in tetrahydrofuran (THF) and the CIP/SSIP ratio appears to be important for achieving efficient Li-doping because of the competing dissociation of the $[NTL]^{\bullet-}$ monoanion radical. However, some questions remain unanswered, and the detailed Li pre-doping mechanism remains unclear.

In this study, we elucidated the mechanism of Li pre-doping of Si using Li–NTL solution by evaluating the effect of the Li concentration in the Li–NTL solution on the physicochemical properties and Li alloying of the Si NE. In organic synthesis, radical monoanions and dianions are formed in Li–NTL solution in THF at different Li concentrations, and the dianions have higher reducing power than the radical monoanions.[36] However, this has not been investigated for Li pre-doping of battery materials because the reaction is driven by monoanions. We expect that dianions will be an important factor for the Li pre-doping reaction of the Si electrode using Li–NTL solution. Here, we prepared Li–NTL solution using MeTHF as the solvent and increased the Li concentration to a Li:naphthalene molar ratio of 2:1 or higher to promote dianionization of naphthalene. To elucidate the mechanism of Li pre-doping of the Si NE, we investigated the effects of the Li concentration on the composition of the Li–NTL

solution, solvation structure, equilibrium potential of the Li–NTL solution, and depth of the Li alloying of the Si NE.

Experimental Section

Preparation of the Li–NTL solutions and Si electrode

The Li–NTL pre-doping solutions were prepared with MeTHF (Sigma-Aldrich Co. LLC) as the solvent, 2.5 mmol naphthalene (Fujifilm Wako Pure Chemical Corporation), and 2.5 mmol, 5.0 mmol, or "saturated" Li (where a substantial amount of Li was added to the solution). Another Li-feeding method, referred to as Li replenishment, was also performed, involving continuous supply of Li by immersing Li foil in the solution during pre-doping. In each case, a 0.5 M Li–NTL solution was prepared in an Ar-filled dry box (MDB-1BK-NT1, Miwa) and stirred overnight.

Si powder comprising spherical particles with diameters of 30–50 nm (Nanostructured & Amorphous Materials, Inc.), Ketjen Black (EC600JD, Lion Corp.), and a polyimide dispersion (Dream Bond, solid ratio of ~46%, I.S.T Corp.) were mixed in *N*-methylpyrrolidone at a solid mass ratio of 80:5:15 to prepare a slurry. This slurry was then coated on a 35-μm-thick Cu foil with a doctor blade, dried in air at 80 °C for 1 h, and dried under vacuum at 200 °C for 12 h. The resulting composite sheet was punched

into disks with a diameter of 16 mm to prepare the Si electrodes. The mass loadings of Si in these electrodes were in the range of 0.38–0.42 mg cm^{-2}.

Li pre-doping using the Li–NTL solutions

An airtight cell (Hohsen Corp.) was used for the Li pre-doping. The cell contained 1.0 mL of the Li–NTL solution, a Si-sheet electrode, a Li foil (to supply the Li–NTL solution with Li^+ ions), and a polyolefin separator (Celgard 2400, Celgard, LLC) between the electrode and Li foil. Each cell was stored at room temperature for 24 h to pre-dope Li into the Si sheet, after which the electrode was removed and rinsed with dimethyl carbonate (DMC, battery grade, Kishida Chemical Co., Ltd.) to remove residual Li–NTL solution.

Electrochemical measurements

CR2032-type coin cells were assembled to prepare Li half-cells. Each coin cell contained a Li-doped Si electrode, a separator (Celgard 3501, Celgard, LLC), a Li metal foil, and an electrolyte solution comprising 1.0 M $LiPF_6$ in an ethylene carbonate (EC):DMC (1:1, v/v, battery grade, Tomiyama Pure Chemical Industries, Ltd.) mixture containing 10 mass% fluoroethylene carbonate (FEC, Tomiyama Pure Chemical

Industries, Ltd.).

The first discharge capacity of each Li pre-doped Si electrode was defined as the Li pre-doping capacity. The discharge capacity measurements were performed at 30 °C in constant-current mode from the open-circuit voltage (OCV_{Si}) to 1.5 V vs. Li/Li^+ at 0.05 mA cm^{-2} current density using a battery tester (HJ1001SD8, Hokuto Denko Corp.).

The charge and discharge tests of the Li half-cells were also performed in constant-current mode at *C*/6 (700 mA g_{Si}^{-1}) between 0.7 and 0.02 V, using a battery tester.

Li air battery (LAB) full cell was assembled in an Ar-filled glove box, by comprising a layer of a lithium metal foil (0.5 mm thick, Honjo Metal) or pre-doped Si NE, a glass microfiber separator (GF/A, Whatman), and an Ketjen Black loaded carbon paper cathode, in a size of φ16 mm (2.0 cm^2 electrode area) inside a gastight cell chamber with gas inlet/outlet valves. The separator and cathode were immersed in 80 μL of electrolyte solution (1 M $LiNO_3$ in tetraethylene glycol dimethylether) before the battery testing. The discharge/charge tests were conducted in current constant mode at 0.2 mA cm^{-2} for 2.5 h with a cycle capacity of 0.5 mAh cm^{-2} (500 mAh g^{-1} per carbon cathode weight) with discharge/charge cutoff voltages of 2.0/4.5 V at 25ºC. Pure oxygen gas was continuously supplied to the gastight cell chamber.

Equilibrium potential measurement of the Li–NTL solutions

The equilibrium potential (V_{eq}) of each Li–NTL solution was assessed from 10 to 30 °C at 2 °C intervals using a two-electrode cell configuration consisting of two compartments. The first compartment contained a Li-metal counter electrode immersed in the same 1.0 M $LiPF_6$/EC+DMC (1:1, v/v) electrolyte solution as that used for the capacity testing (except for the absence of FEC). The second compartment consisted of a Ni-mesh working electrode and 0.5 M Li–NTL solution. The two compartments were separated by a Li^+-conductive solid electrolyte plate made of $Li_7La_3Zr_2O_{12}$ (Toshima Manufacturing Co., Ltd.) to prevent the two solutions from mixing without losing the Li^+-ion conduction.

Spectroscopic analysis of the Li-NTL solutions

The changes in structure of NTL, that is, the formation and amounts of the $NTL^{\bullet-}$ monoanion radical and NTL^{2-} dianion, in the Li–NTL solutions were investigated by a Fourier transform infra-red (FT-IR) spectrometer (FT-IR-4100, JASCO Corp.) used in an attenuated total reflection (ATR) method. Approximately 200 μL Li-NTL solutions were dropped onto the diamond prism (optical path length = 0.2 mm) and the lid was closed under an Ar atmosphere. The measurement range was the fingerprint area (600 to 1000 cm^{-1}).

The state of NTL, that is, the formation and amounts of the $NTL^{\bullet-}$ monoanion radical and NTL^{2-} dianion, in the Li–NTL solutions were evaluated by ultraviolet–visible (UV–vis) spectroscopy (V-6500ST, JASCO Corp.). Each sample was placed into glass cell (optical path length = 0.2 mm) and the UV–vis spectrum of the sample was obtained at room temperature. The baseline spectrum of each solvent was subtracted from the sample spectrum.

Characterization of Si NEs

The changes in the Si crystal structure induced by Li pre-doping were identified by Automated Multipurpose X-ray Diffractometer (XRD) (UltimaIV, Rigaku Corp.) using Cu-*K*α radiation (40 kV, 50 mA). All measurements were performed using a non-exposed cell (manufactured by Rigaku) to prevent exposure of the Si NE to the atmosphere.

The morphology of Si NE before and after Li Pre-doping was observed and analyzed by scanning electron microscopy (SEM, JSM-7800F, JEOL) and energy dispersive X-ray spectroscopy (EDS, X-MAX^N, Oxford) equipped with the SEM. After Li pre-doping, Si NEs were taken out from the chamber and rinsed DMC solvent one time in an Ar-filled glove box.

Highest occupied molecular orbital energies

The highest occupied molecular orbital (HOMO) energies were calculated based on structural optimization of each molecule and ion in vacuum by density functional theory (DFT) with the B3LYP exchange–correlation functional and 6-311G(d, p) basis set.[37]

Results and Discussion

Composition analysis and physical property evaluation of the Li–NTL solutions

To investigate the compositional changes of the Li–NTL solutions with different Li concentrations, the solutions were analyzed by Fourier transform infrared (FTIR) spectroscopy. The FTIR spectra of the Li–NTL solutions with different Li concentrations are shown in Fig. 1. There are two notable absorption peaks in the FTIR spectra: the first peak at 970 cm^{-1} is attributed to the C–H in-plane bending vibration and the second peak at 687 cm^{-1} is attributed to the C–H out-of-plane bending and aromatic ring C–C vibrations.[28,38] Both signals are representative absorption peaks of naphthalene dianions that receive two electrons by reduction owing to Li metal in the solution. The changes in the absorption signals suggest that the dipole moment in the naphthalene molecule changed because of the formation of an ion pair with two Li^+ ions. The other signals at 998 and 740 cm^{-1} are common absorptions for the monoanions and dianions, indicating

that the total amount of anions increases depending on the Li concentration. In addition, the signal intensities increased with increasing Li concentration, indicating that dianion formation increased with increasing Li concentration.

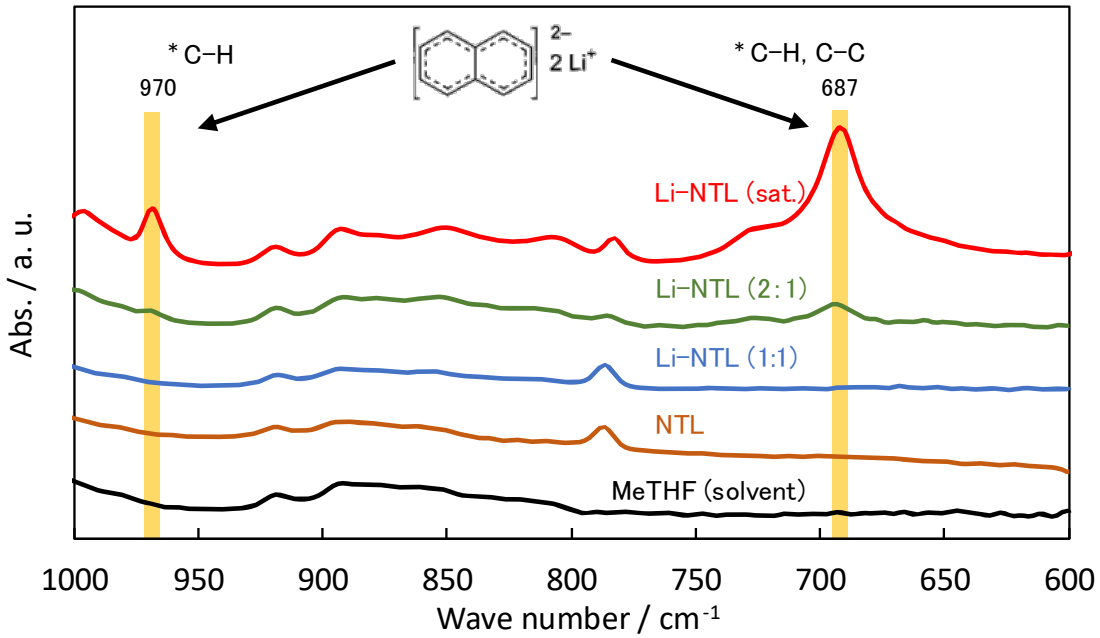

Figure 1. Fourier transform infrared spectra of the Li–naphthalenide (NTL) solutions with different Li concentrations.

UV–vis spectroscopy was performed to analyze the compositional changes of the Li–NTL solution with increasing Li concentration in more detail. The UV–vis spectra of the Li–NTL solutions with different Li concentrations are shown in Fig. 2. There are two points to note. The first point is the absorption signal at approximately 550 nm. This signal

corresponds to the dianion, and its intensity increased with increasing Li concentration.[39,40] The results obtained by comparing the area ratios of these absorption signals and evaluating the amount of the dianion are given in Table S1. The peak area attributed to the dianion in the saturated Li–NTL solution was approximately three times larger than that in the Li–NTL solution with a 1:1 molar ratio. Here, the dianion forms a CIP with two Li^+ ions.[41] The second point to note is the absorption signal at approximately 320 nm. This signal is attributed to the monoanion, and there were two peaks for the 1:1 Li–NTL solution. There are two main types of monoanion structures, that is, the CIP type at relatively low wavelength and the SSIP type at relatively high wavelength. For both types of monoanion structure, the $NTL^{\bullet-}$ radical monoanions form ion pairs with one Li^+ ion.[42] The CIP and SSIP coordination structures are shown in Fig. 2. The cation and anion are in direct contact, so the CIP is relatively stable owing to the strong Coulomb force. In contrast, the SSIP has high reactivity. The CIP/SSIP ratio depends on the type of solvent, and the CIP and SSIP coexist in Li–NTL using MeTHF as the solvent.[34] By increasing the Li concentration, the intensities of both monoanions decreased, and the CIP signal disappeared for the 2:1 Li–NTL solution. Furthermore, both monoanion signals disappeared for the saturated Li–NTL solution. These monoanions and dianion are in equilibrium according to the following equation:[42,43]

$$2\mathrm{Li} + 2\mathrm{NTL} \rightleftarrows 2\mathrm{Li}^{+}[\mathrm{NTL}^{\cdot -}]$$

$$\rightleftarrows \mathrm{NTL} + \mathrm{Li}_2^{+}[\mathrm{NTL}^{2-}] \qquad (1)$$

According to Le Chatelier's principle, the direction of this equilibrium reaction shifts toward formation of the dianion as the Li concentration increases, resulting in an increase in the dianion concentration. This coincides with the Li^+ concentrations in the Li–NTL solutions measured by ion chromatography (Table S2). However, the formation of the dianion also promoted byproduct formation (Fig. S2),[36] which is indicated by the signal at approximately 425 nm.

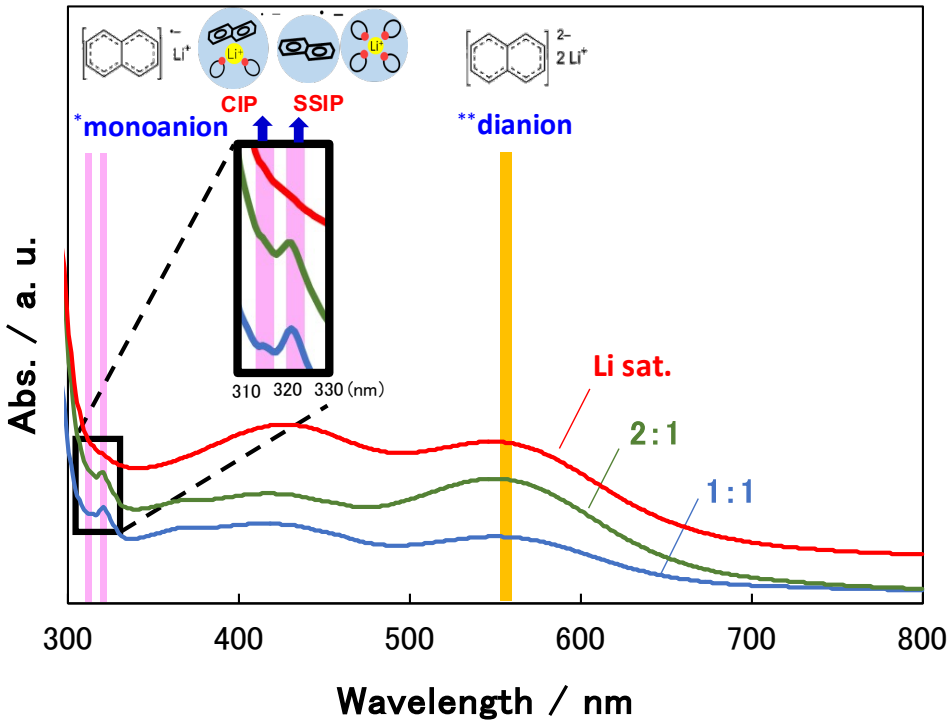

Figure 2. Ultraviolet–visible spectra of the Li–NTL solutions with different Li concentrations.

The formation and stability of the dianion were evaluated to clarify the characteristics of the radical anions in the Li–NTL solutions. The UV–vis spectra of the saturated Li–NTL solution with Li metal at different times are shown in Fig. S1, showing the rate of dianion formation. The results indicated that the dianion began to form within 5 min of the start of stirring, and the concentration of the dianion reached a maximum after 30 min. Li and naphthalene rapidly reacted with the addition of Li metal to the solution to form ion pairs. In contrast, the intensity in the region of 425 nm increased with time. This suggests that byproducts were generated by the reaction of a trace amount of water in the Ar-filled dry box with the Li–NTL solution (Fig. S2).[36] It is conceivable that these byproducts inhibit the Li pre-doping reaction. Therefore, the stirring time is a very important factor for the Li pre-doping reaction to prepare an active Li–NTL solution. The UV–vis spectra of the saturated Li–NTL solution without Li metal at different times are shown in Fig. S3, showing the rate of dianion generation and the stability of the dianion. The intensity of the spectrum sharply decreased with time, and the dianion signal at approximately 550 nm decreased by 94% when the Li–NTL solution was allowed to stand

for 24 h compared with after standing for 1 h. In addition, the monoanion signal at 320 nm reappeared after standing for 1, 3 and 5 h. This suggests that the equilibrium between the monoanion and dianion shown in Equation (1) gradually shifted toward the monoanion.

We then measured the equilibrium potentials of the Li–NTL solutions with different Li concentrations. The equilibrium potential of the solution is an important factor to evaluate the Li pre-doping ability because the Li pre-doping reaction does not proceed if the equilibrium potential of the Li–NTL solution is higher than the electrochemical Li alloying potential of the Si electrode. The equilibrium potentials of the Li–NTL solutions with different Li concentrations as a function of the temperature are shown in Fig. 3. The equilibrium potential of the Li–NTL solution was lowering as the Li concentration increased. The potential of the Li–NTL solution under the Li-replenishment condition was achieved below 0.1 V vs. Li/Li^+ of the electrochemical Li alloying potential of the Si electrode, suggesting that the Li pre-doping reaction proceeded owing to the generation of the fresh dianion from naphthalene. In addition, the potential of the Li–NTL solution was also lowering as the temperature increased. This is because the reaction rate of radical species increases with increasing temperature. These results suggest that the monoanion and dianion were in equilibrium in the Li–NTL solution. The equilibrium equations are

given by

$$\mathrm{Li(s) + NTL + 4(solvent) \rightleftarrows (solvent)_4Li^+[NTL]^{\cdot -}} \\ \rightleftarrows \mathrm{(solvent)_2Li^+[NTL]^{\cdot -} + 2(solvent)} \quad (2)$$

$$\mathrm{Li(s) + 2(solvent) + (solvent)_2Li^+[NTL]^{\cdot -}} \\ \rightleftarrows \mathrm{(solvent)_2Li^+[NTL]^{2-}Li^+(solvent)_2} \quad (3)$$

In the Li–NTL solution using the MeTHF solvent with a constantly saturated Li concentration, the solution composition was predominantly that of the reaction given by Equation (3), resulting in the presence of a large amount of dianions. In contrast, in the Li–NTL solutions with insufficient Li concentrations, the dianion formation did not sufficiently proceed owing to the lack of monoanions. Therefore, the proportion of dianions decreased and the proportion of monoanions increased, causing a higher apparent equilibrium potential. However, there were still some dianions in the solution, so the Li pre-doping reaction proceeded to some extent.

The structures of the monoanion and dianion were optimized by DFT (Fig. S4). The HOMO energies of the Li–NTL and Li_2–NTL ion pairs are −1.87 and −1.59 eV, respectively. The HOMO energy of the dianion is higher than that of the monoanion, indicating that the reducing power of the dianion is also higher than that of the monoanion. Moreover, a cluster structure consisting of a disordered arrangement of many solvated Li ions and naphthalene dianions also forms under the high Li concentration.[44] This is

consistent with the change in the composition of the Li–NTL obtained from the UV–vis spectra and the lowering of the equilibrium potential, and it suggests that the generation of dianions with high reducing power lowers the equilibrium potential of the Li–NTL solution.

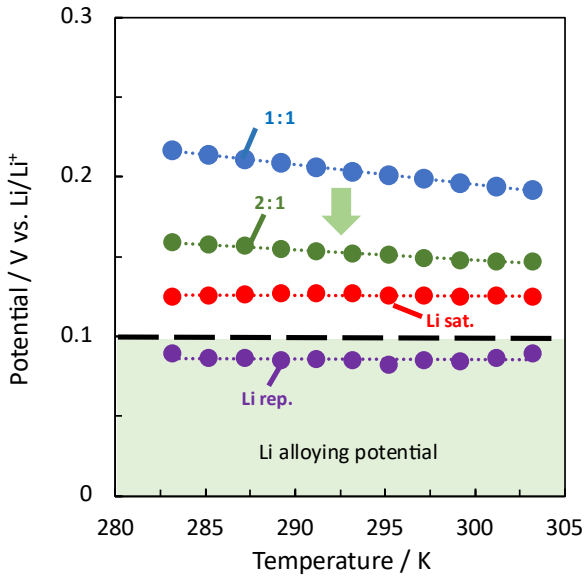

Figure 3. Equilibrium potentials of 0.5 M Li–NTL solutions with various Li concentrations as a function of the temperature.

Evaluation of the Li pre-doping abilities of the Li–NTL solutions with different Li concentrations

To evaluate the Li pre-doping abilities of the Li–NTL solutions with different Li concentrations, Si electrodes were pre-doped for 24 h using the Li–NTL solutions and the amount of Li pre-doping was compared with the initial capacity. The first discharge

curves are shown in Fig. 4. The capacity, indicating the amount of Li pre-doping, increased as the Li concentration increased. The capacity under the Li-replenishment condition (2888 mAh g^{-1}) was significantly higher than those under the other conditions. To analyze this effect in detail, the dQ/dV curves were obtained by differentiating the discharge curves with respect to the voltage (Fig. S5). The peak of Li de-alloying from the $Li_{3.75}Si$ crystal phase,[45,46] which is the deepest Li alloyed phase, was observed at approximately 0.4 V under the Li-replenishment condition. No such peak was observed under the other conditions, suggesting that deep Li pre-doping did not occur. The equation of the Li pre-doping reaction suggested by these results is

$$x[(\text{solvent})_2\text{Li}^+[\text{NTL}]^{2-}\text{Li}^+(\text{solvent})_2] + \text{Si} \longrightarrow \text{Li}_x\text{Si} + x(\text{solvent})_2\text{Li}^+[\text{NTL}]^{\cdot-} + 2x(\text{solvent}) \quad (4)$$

In Li–NTL solution, naphthalene forms a dianion owing to the high Li concentration, which lowers the equilibrium potential of the solution and transfers electrons to Si. It is inferred that Si is negatively charged by the reduction of Si, and then Li pre-doping occurs as a result of the Si undergoing an alloying reaction with Li^+ ions. The amount of Li pre-doping showed the highest capacity under the Li-replenishment condition. This was caused by repeating the following reaction during Li pre-doping: naphthalene and the monoanion were reduced by Li metal, which became a monoanion and a dianion to form

an ion pair, and the Li pre-doping reaction occurred as shown in Equation (4).

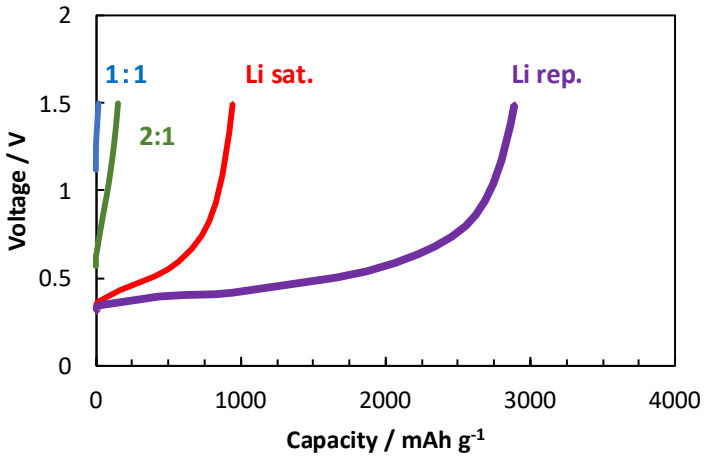

Figure 4. First discharge curves of the Li pre-doped Si electrodes with Li–NTL solutions at different Li concentrations.

Characterization of the Li pre-doped Si electrodes

To investigate the effect of Li pre-doping on the Si electrode, the particle size of Si and elemental composition of the Si electrode surface were analyzed before and after Li pre-doping. Scanning electron microscopy (SEM) images of the Si particles on the electrode before and after Li pre-doping under each Li concentration are shown in Fig. 5a–e. The Si particle size increased from 40 to 130 nm by Li pre-doping, and it depended on the Li concentration in the Li–NTL solution. In addition, energy-dispersive spectroscopy (EDS) analysis of Si (Fig. 5f–j) confirmed that the elemental proportion of Si decreased as the Li concentration of the Li–NTL solution increased, indicating that the rate of the Li pre-

doping reaction increased as the Li concentration increased.

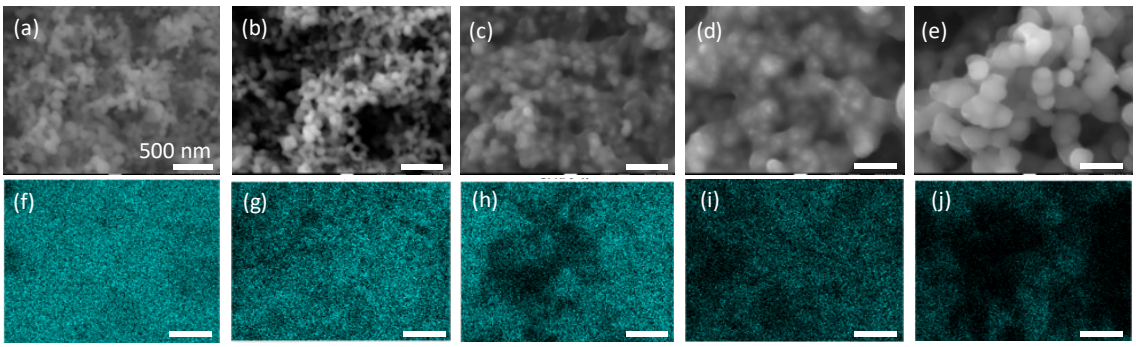

Figure 5. Scanning electron microscopy images and energy-dispersive spectroscopy maps of the Li pre-doped Si electrode surfaces. Scanning electron microscopy images of (a) pristine Si and (b)–(e) Li pre-doped Si under 1:1 molar ratio, 1:2 molar ratio, Li-saturated, and Li-replenishment conditions of the Li–NTL solution, respectively. Si EDS maps of (f) pristine Si and (g)–(j) Li pre-doped Si under 1:1 molar ratio, 1:2 molar ratio, Li-saturated, and Li-replenishment conditions of the Li–NTL solution, respectively.

To determine the crystal structure change of Si by Li pre-doping, the Li pre-doped Si electrodes were analyzed by XRD. The XRD spectra of the Si electrodes before and after Li pre-doping using Li–NTL solutions with different Li concentrations are shown in Fig. 6. The diffraction peak of the Si crystalline phase disappeared as the Li concentration of the Li–NTL solution increased owing to Li pre-doping. The diffraction peaks of the (220) and (332) planes of the $Li_{3.75}Si$ phaseb[47] were clearly observed for the Li pre-doped Si

electrode under the Li-replenishment condition, but the (110) Si diffraction peak completely disappeared. This suggests that crystalline Si was destroyed and became amorphous Si as a result of Li pre-doping.

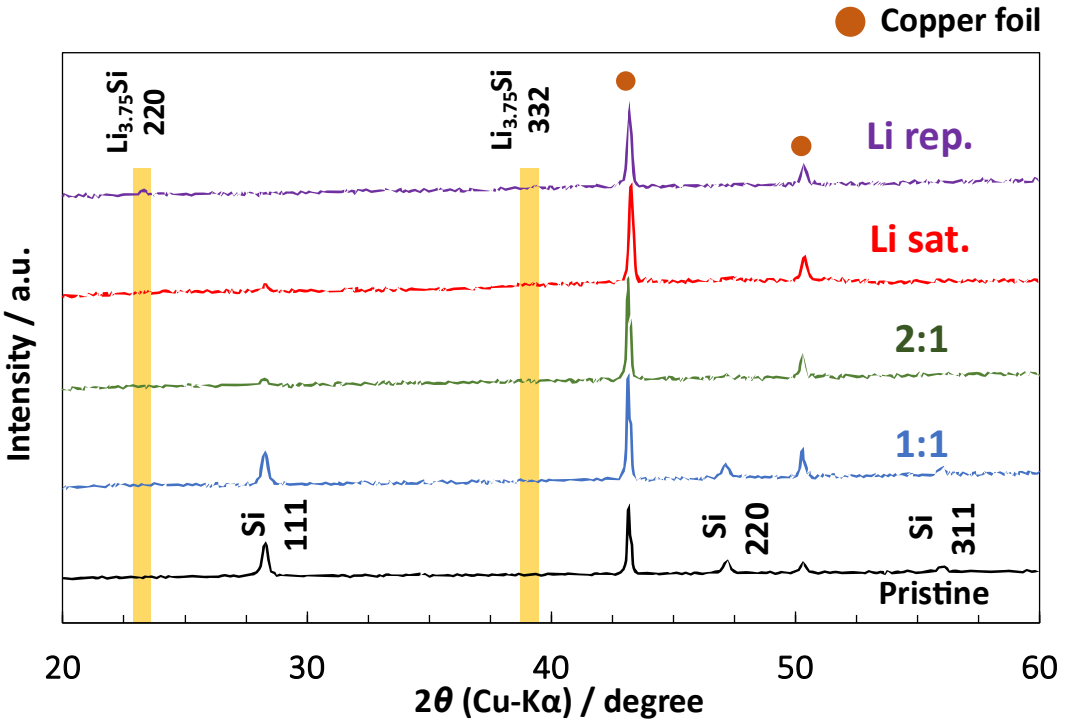

Figure 6. X-ray diffraction patterns of the Li pre-doped Si electrodes with Li–NTL solutions at different Li concentrations.

Electrochemical performance of Li half-cells

The effects of the Li pre-doping process on the Li alloying behavior were investigated by comparing the electrochemical performance of the pristine Si and Li pre-doped Si

electrodes under Li replenishment of the Li-NTL solution using Li half-cells under the same conditions. The charge–discharge curves of the Li half-cells using the pristine Si and Li pre-doped Si electrodes are shown in Fig. 7a and b, respectively. The charge–discharge reaction normally occurred. The charge–discharge curves did not change with the Li pre-doping process, indicating that Li pre-doping did not have an adverse effect on subsequent charge–discharge cycles. In addition, the initial irreversible capacity was observed for the pristine Si electrode, which indicates that a large amount of charging capacity was lost by electrolyte solution decomposition and subsequent solid–electrolyte interphase film formation during the first charging cycle. In contrast, the initial irreversible capacity was not observed for the Li pre-doped Si electrode, suggesting that the reaction did not occur. This phenomenon is consistent with the change in Si particle size (Fig. S6) and cell resistance (Fig. S7) after 1st charging. The discharge cycle performance and coulombic efficiency in the charge–discharge tests are shown in Fig. 7c and d, respectively. The cell containing the Li pre-doped Si electrode maintained a high discharge capacity for approximately 70 cycles. Li pre-doping eliminated the initial low coulombic efficiency and maintained the capacity retention above 95%. By Li pre-doping, the crystal structure of Si was disrupted and the $Li_{3.75}Si$ crystalline phase was formed. During discharge, the occurrence of de-alloying by phase transfer from the $Li_{3.75}Si$

crystalline phase to the Li_xSi amorphous phase, resulting that Li ions easier inserts into the pre-doped Si NE compared to pristine Si NE. In addition, the volume change of the Li pre-doped Si NE was sufficiently smaller than pristine Si NE, and serious damage, such as cracking and crushing, was successfully prevented.[13,23] These results confirm that our Li pre-doping is effective for reducing the initial irreversible capacity and improving the cycle performance. Furthermore, the LAB full cell with the pre-doped Si NE showed good charge and discharge performance equivalent to those using Li metal NE (Fig. S8).

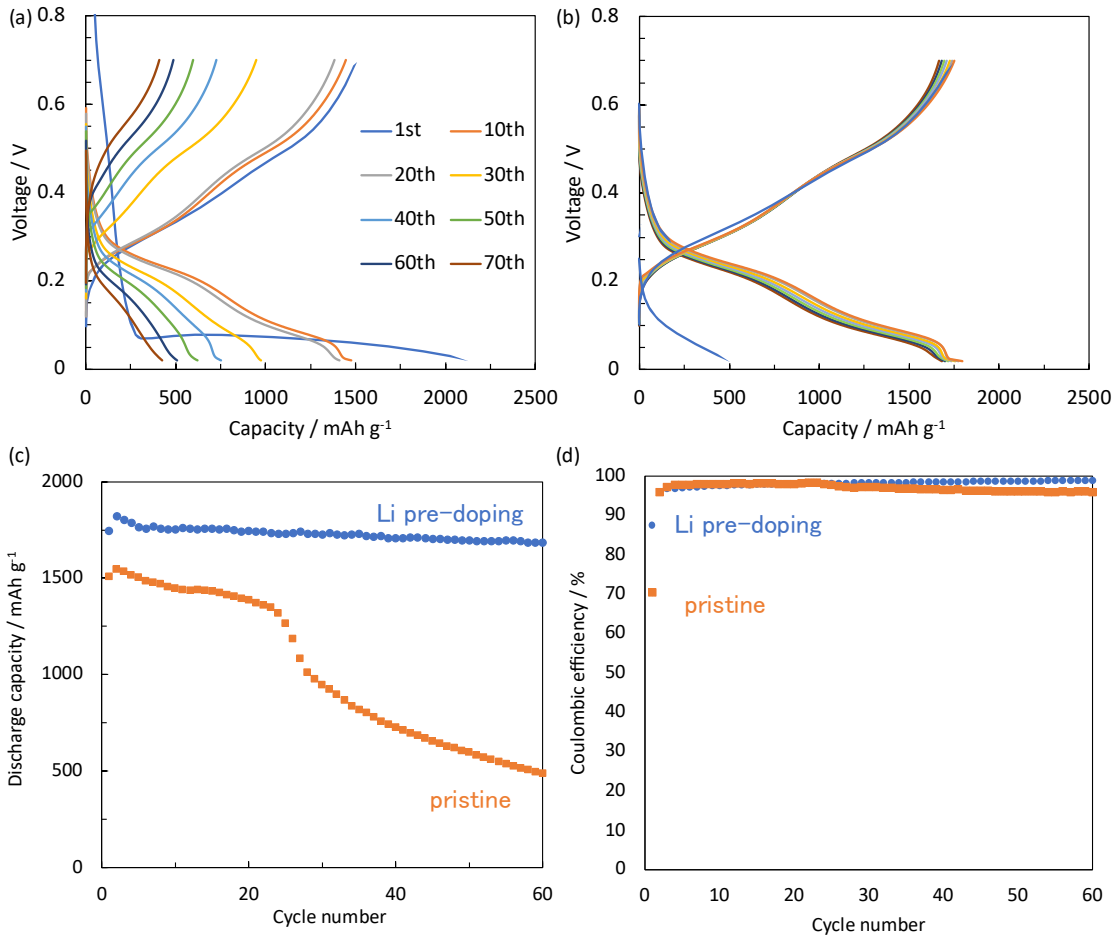

Figure 7. Electrochemical performance of the pristine Si and Li pre-doped Si electrode

using Li half-cells. Charge–discharge curves of the (a) pristine Si and (b) Li pre-doped Si electrodes. (c) Cycle performance and (d) coulombic efficiency of the pristine Si and Li pre-doped Si electrodes in the charge–discharge test.

Conclusions

In this study, we investigated the effect of the Li concentration of the Li–NTL solution on the mechanism of Li pre-doping of Si. We found that radical dianions are generated in the Li–NTL solution by increasing the Li concentration, which lowers the equilibrium potential of the Li–NTL solution and promotes the Li pre-doping of the Si electrode. The Li pre-doping capacity depends on the Li concentration of the Li–NTL solution. The highest capacity of ~3000 mAh g^{-1} was comparable with the theoretical capacity of Si under Li-replenishment conditions. This behavior resulted from the solvation structure of the Li–NTL solution. Even during electrochemical charging and discharging, the solvation structure of the electrolyte greatly affects the Li intercalation reaction into Si electrode.[48] Analysis of the solvation structure by FTIR and UV–vis spectroscopy indicated that the Li–NTL solutions with high Li concentrations contained large amounts of dianions as the key component for Li pre-doping. The Li pre-doping capacity is determined by the equilibrium potential of the Li–NTL solution because of the

equilibrium formation of ion pairs of the solvated Li^+ ions, $[NTL]^{\bullet-}$ radical monoanions, and $[NTL]^{2\bullet-}$ radical dianions. Based on these results, Li pre-doping using Li–NTL solution under Li-replenishment conditions repeatedly causes the following Li pre-doping reaction: naphthalene reacts with the Li metal, the radical monoanion and dianion form, and then an ion pair forms, resulting in Li pre-doping of the Si electrode (Fig. 8). High Li pre-doping can be achieved by repeating this cycle. Furthermore, the electrochemical performance using the Li-pre-doped Si electrode revealed that Li pre-doping is also effective for reducing the initial irreversible capacity and improving the cycle performance.

Here, we proposed that Si can be more deeply pre-doped by increasing the proportion of dianions in the pre-doping solution. We anticipate that the development of deeper and faster pre-doping technology can be achieved by exploring solvents and aromatic compounds that promote the generation of dianions. In addition, we believe that the Li pre-doping chemical reaction, including dianions, is applicable to a wide range of electrode materials, not only to the Si NE, but also to various NE materials, such as hard carbon, SiO, and Sn, and positive electrode materials, such as sulfur, which will improve the chemistry of next-generation batteries such as Li-S and Li-Air battery.

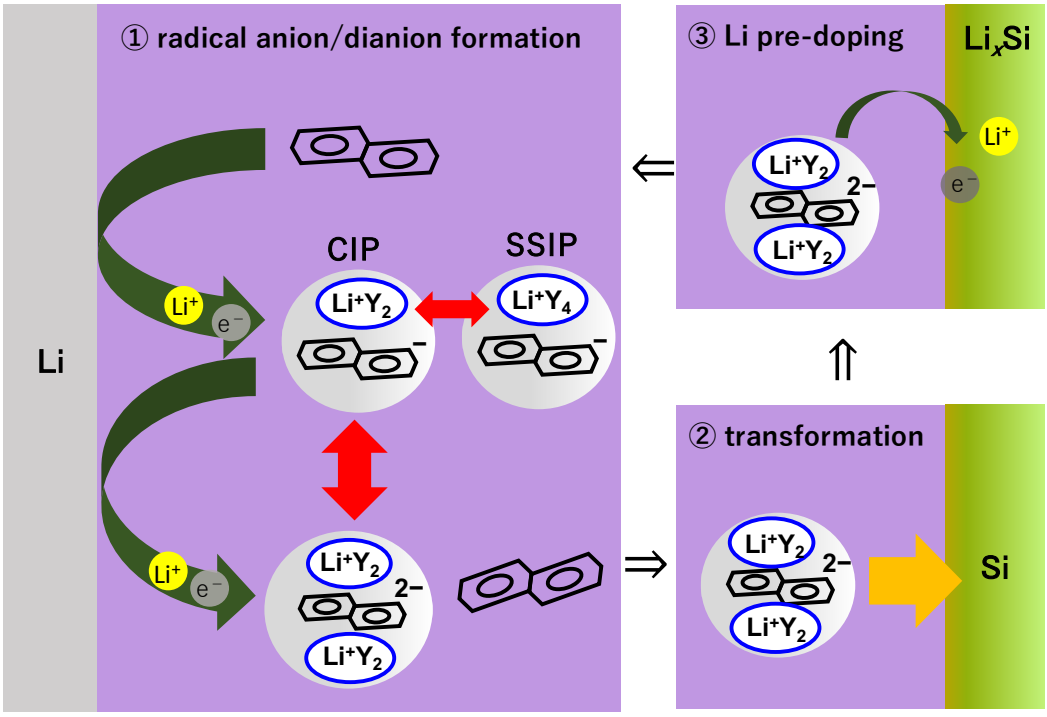

Figure 8. Reaction mechanism of Li pre-doping using Li–NTL solution with constantly saturated Li concentration. (Y = MeTHF)

Supporting Information

Li^+ concentrations in Li–NTL solutions; Resistances obtained from circuit fitting; Additional UV-Vis spectra of Li–NTL solutions; Byproduct generation reaction; DFT-optimized molecular structures; DQ/DV plots; SEM images of Si electrodes; Nyquist plots; Discharge/Charge curve of Li Air Battery

Acknowledgments

This work was partially supported by a project of the Center for Asian and Pacific

Studies, Seikei University, Japan, research grants for FY2024 (first half of the year) Amano Institute of Technology Public Interest Foundation, and the National Institute for Materials Science (NIMS) Joint Research Hub Program. The SEM–EDS measurements were performed at the NIMS Battery Research Platform. We thank Edanz for editing a draft of this manuscript.

References

1. Van Noorden, R.; "Sulphur back in vogue for batteries", *Nature* 2013, **498**, 416–417. https://doi.org/10.1038/498416a
2. Song, C. L.; Li, G. H.; Yang, Y.; Hong, X. J.; Huang, S.; Zheng, Q. F.; Si, L. P.; Zhang, M.; Cai, Y. P.; "3D catalytic MOF-based nanocomposite as separator coatings for high-performance Li-S battery", *Chem. Eng. J.* 2020, **381**, 122701. https://doi.org/10.1016/j.cej.2019.122701
3. Liu, B.; Bo, R.; Taheri, M.; Di Bernardo, I.; Motta, N.; Chen, H.; Tsuzuki, T.; Yu, G.; Tricoli, A.; "Metal–Organic Frameworks/Conducting Polymer Hydrogel Integrated Three-Dimensional Free-Standing Monoliths as Ultrahigh Loading Li–S Battery Electrodes", *Nano Lett.* 2019, **19**, 4391–4399. https://doi.org/10.1021/acs.nanolett.9b01033
4. Huang, J. Q.; Zhuang, T. Z.; Zhang, Q. H.; Peng, J.; Chen, C. M.; Wei, F.; "Permselective Graphene Oxide Membrane for Highly Stable and Anti-Self-Discharge Lithium–Sulfur Batteries" *ACS Nano* 2015, **9**, 3002–3011. https://doi.org/10.1021/nn507178a
5. Nomura, A.; Ito, K.; Kubo, Y.; "CNT Sheet Air Electrode for the Development of Ultra-High Cell Capacity in Lithium-Air Batteries", *Sci. Rep.* 2017, **7**, 45596. https://doi.org/10.1038/srep45596
6. Hayashi, Y.; Honda, R.; Moro, I.; Fukunishi, M.; Otsuka, H.; Kubo, Y.; Horiba, T.; Saito, M.; "LiBr-coated Air Electrodes for Li-air Batteries", *Electrochemistry* 2021, **89**, 557–561. https://doi.org/10.5796/electrochemistry.21-00096
7. Hayashi, Y. ; Yamada, S.; Ishikawa, T.; Takamuki, Y.; Sohmiya, M.; Otsuska, H.; Ito, K.; Kubo, Y.; Saito, M.; "Enhancement of Bifunctional Effect for $LiNO_3$/glyme Electrolyte by Using Dual Solvent System for Li-O_2 Batteries", *J. Electrochem. Soc.* 2020, **167**, 020542. https://doi.org/10.1149/1945-7111/ab6975

8. Saito, M.; Fujinami, T.; Sohmiya, M.; Hayashi, Y.; Koyama, K.; Otsuka, H.; Ito, K.; Kubo, Y.; Horiba, T.; "Comparison of Lithium Salt Effect on Negative Electrodes and Lithium–Air Cell Performance", *J. Electrochem. Soc.*, **168**, 010520 (2021). https://doi.org/10.1149/1945-7111/abd60d
9. Hassoun, J.; Scrosati, B.; "Review—Advances in Anode and Electrolyte Materials for the Progress of Lithium-Ion and beyond Lithium-Ion Batteries", *J. Electrochem. Soc.* 2015, **162**, A2582. https://doi.org/10.1149/2.0191514jes
10. Domi, Y.; Usui, H.; Iwanari, D.; Sakaguchi, H.; "Advanced Performance of Annealed Ni–P/(Etched Si) Negative Electrodes for Lithium–Ion Batteries", *J. Electrochem. Soc.* 2017, **164**, A1651–A1654. https://doi.org/10.1149/2.1211713jes
11. Saito, M.; Kato, K.; Ishii, S.; Yoshii, K.; Shikano, M.; Sakaebe, H.; Kiuchi, H.; Fukunaga, T.; Matsubara, E.; "Effective Bulk Activation and Interphase Stabilization of Silicon Negative Electrode by Lithium Pre-Doping for Next-Generation Batteries", *J. Electrochem. Soc.* 2019, **166**, A5174–A5183. https://doi.org/10.1149/2.0271903jes
12. Long, B. R.; Chan, M. K. Y.; Greeley, J. P.; Gewirth, A. A.; "Dopant Modulated Li Insertion in Si for Battery Anodes: Theory and Experiment", *J. Phys. Chem. C* 2011, **115**, 18916–18921. https://doi.org/10.1021/jp2060602
13. Wang, Y.; Satoh, M.; Arao, M.; Matsumoto, M.; Imai, H.; Nishihara, H.; "Long-cycle-life Secondary Battery with Electrochemically Pre-doped Silicon Anode", *Sci. Rep.* 2020, **10**, 3208. https://doi.org/10.1038/s41598-020-59913-4
14. Wen, C. J.; Huggins, R. A.; "Chemical diffusion in intermediate phases in the lithium-tin system", *J. Solid State Chem* 1980, **35**, 376–384. https://doi.org/10.1016/0022-4596(80)90535-6
15. Liu, X. H.; Wang, J. W.; Huang, S.; Fan, F.: Huang, X.; Liu, Y.; Krylyuk, S.; Yoo, J.; Dayeh, S. A.; Davydov, A. V.; Mao, S. X.; Picraux, S. T.; Zhang, S.; Li, J.; Zhu, T.; Huang, J. Y.; "In situ atomic-scale imaging of electrochemical lithiation in silicon", *Nat. Nanotechnol.* 2012, **7**, 749–756. https://doi.org/10.1038/nnano.2012.170
16. Pharr, M.; Zhao, K.; Wang, X.; Suo, Z.; Vlassak, J. J.; "Kinetics of Initial Lithiation of Crystalline Silicon Electrodes of Lithium-Ion Batteries", *Nano Lett.* 2012, **12**, 5039–5047. https://doi.org/10.1021/nl302841y
17. Holtstiege, F.; Bärmann, P.; Nölle, R.; Winter, M.; Placke, T.; "Pre-Lithiation Strategies for Rechargeable Energy Storage Technologies: Concepts, Promises and Challenges", *Batteries* 2018, **4**, 4. https://doi.org/10.3390/batteries4010004
18. Sethuraman, V. A.; Chon, M. J.; Shimshak, M.; Srinivasan, V.; Guduru, P. R.; "In Situ Measurements of Stress Evolution in Silicon Thin Films During Electrochemical Lithiation and Delithiation", *J. Power Sources.* 2010, **195**, 5062.

https://doi.org/10.1016/j.jpowsour.2010.02.013

19. Chan, M. K. Y.; Long, B. R.; Gewirth, A. A.; Greeley, J. P.; "The First-Cycle Electrochemical Lithiation of Crystalline Ge: Dopant and Orientation Dependence and Comparison with Si", *J. Physic. Chem. Lett.* 2011, **2**, 3092. https://doi.org/10.1021/jz201432d
20. He, W.; Xu, H.; Chen, Z.; Long, J.; Zhang, J.; Jiang, J.; Dou, H.; Zhang, X; "Regulating the Solvation Structure of Li^+ Enables Chemical Prelithiation of Silicon-Based Anodes Toward High-Energy Lithium-Ion Batteries", *Nano-Micro Lett.* 2023, **15**, 107. https://doi.org/10.1007/s40820-023-01068-8
21. Shellikeri, A.; Watson, V. G.; Adams, D. L.; Kalu, E. E.; Read, J. A.; Jow, T. R.; Zheng, J. P.; "Pre-Lithiation of Carbon Anodes Using Different Lithium - Sources", *ECS Trans.* 2017, **77**, 293. https://doi.org/10.1149/07711.0293ecst
22. Jarvis, C. R.; Lain, M. J.; Yakovleva, M. V.; Gao, Y.; "A prelithiated carbon anode for lithium-ion battery applications", *J. Power Sources* 2006, **162**, 800-802. https://doi.org/10.1016/j.jpowsour.2005.07.051
23. Okubo, T.; Saito, M.; Yodoya, C.; Kamei, A.; Hirota, M.; Takenaka, T.; Okumura, T.; Tasaka, A.; Inaba, M.; "Effects of Li pre-doping on charge/discharge properties of Si thin flakes as a negative electrode for Li-ion batteries", *Solid State Ionics* 2014, **262**, 39-42. https://doi.org/10.1016/j.ssi.2013.09.014
24. Liu, N.; Hu, L.; McDowell, M. T.; Jackson, A.; Cui, Y.; "Prelithiated silicon nanowires as an anode for lithium ion batteries", *ACS Nano* 2011, **5**, 6487-6493. https://doi.org/10.1021/nn2017167
25. Abe, T.; Mizutani, Y.; Tabuchi, T.; Ikeda, K.; Asano, M.; Harada, T.; Inaba, M.; Ogumi, Z.; "Intercalation of lithium into natural graphite flakes and heat-treated polyimide films in ether-type solvents by chemical method", *J. Power Sources* 1997, **68**, 216-220. https://doi.org/10.1016/S0378-7753(96)02554-2
26. Yoshida, S. ; Masuo, Y.; Shibata, D.; Haruta, M.; Doi, T.; Inaba, M.; "Li Pre-doping of Amorphous Silicon Electrode in Li-Naphthalene Complex Solutions", *Electrochemistry* 2015, **83**, 843–845. https://doi.org/10.5796/electrochemistry.83.843
27. Wang, G.; Li, F.; Liu, D.; Zheng, D.; Luo, Y.; Qu, D.; Ding, T.; Qu, D.; "Chemical Prelithiation of Negative Electrodes in Ambient Air for Advanced Lithium-Ion Batteries", *ACS Appl. Mater. Interfaces* 2019, **11**, 8699–8703. https://doi.org/10.1021/acsami.8b19416
28. Tan, K. S.; Yazami, R.; "Physical-Chemical and Electrochemical Studies of the Lithium Naphthalenide Anolyte", *Electrochim. Acta* 2015, **180**, 629–635. https://doi.org/10.1016/j.electacta.2015.07.100
29. Lunchev, A. V.; Tan, K. S.; Grimsdale, A. C.; Yazami, R.; "Electrical and electrochemical

properties of lithium solvated electron solutions derived from 1,3,5-triphenylbenzenes", *New J. Chem.* 2018, **42**, 15678–15683. http://dx.doi.org/10.1039/C8NJ03362E

30. Tan, K. S.; Grimsdale, A. C.; Yazami, R.; "Synthesis and Characterization of Biphenyl-Based Lithium Solvated Electron Solutions", *J. Phys. Chem. B* 2012, **116**, 9056–9060. https://doi.org/10.1021/jp302160a
31. Lunchev, A. V.; Liu, Z.; Su, H.; Yazami, R.; Grimsdale, A. C.; "Electrical and electrochemical properties of triphenylene based lithium solvated electron solutions", *Electrochim. Acta* 2018, **292**, 142–146. https://doi.org/10.1016/j.electacta.2018.09.130
32. Lunchev, A. V.; Liu, Z.; Li, W.; Ruan, S.; Su, H.; Yazami, R.; Grimsdale, A. C.; "Electrochemical properties of p-terphenyl based lithium solvated electron solutions", *J. Electroanal. Chem.* 2020, **875**, 114148. https://doi.org/10.1016/j.jelechem.2020.114148
33. Inamoto, J.; Maruyama, S.; Matsuo, Y.; Uchida, S.; Maeda, K.; Ishikawa, M.; "Effects of Pre-Lithiation on the Electrochemical Properties of Graphene-Like Graphite", *Electrochemistry* 2019, **87**, 260–264. https://doi.org/10.5796/electrochemistry.19-00027
34. Fukunishi, M.; Ishii, S.; Himata, Y.; Kondo, A.; Ozawa, F.; Saito, M. ; "Li Pre-Doping into Si Negative Electrodes Using Li-Naphthalenide Solutions with Various Ether Solvents For Next-Generation Batteries", *J. Electrochem. Soc.* 2022, **169**, 060534. https://doi.org/10.1149/1945-7111/ac7673
35. Shen, Y.; Shen, X.; Yang, M.; Qian, J.; Cao, Y.; Yang, H.; Luo, Y.; Ai, X.; "Achieving Desirable Initial Coulombic Efficiencies and Full Capacity Utilization of Li-Ion Batteries by Chemical Prelithiation of Graphite Anode", *Adv. Funct. Mater.* 2021, **31**, 1–9. https://doi.org/10.1002/adfm.202101181
36. Yus, M.; Herrera, R. P.; Guijarro, A.; "On the Mechanism of Arene-Catalyzed Lithiation: The Role of Arene Dianions—Naphthalene Radical Anion versus Naphthalene Dianion", *Chem. - A Eur. J.* 2002, **8**, 2574–2584. https://doi.org/10.1002/1521-3765(20020603)8:11%3C2574::AID-CHEM2574%3E3.0.CO;2-K
37. Saito, M.; Hayamizu, K.; Okada, T.; "Temperature dependence of ion and water transport in perfluorinated ionomer membranes for fuel cells", *J. Physic. Chem. B* 2005, **109**, 3112. https://doi.org/10.1021/jp045624w
38. Lippincott, E. R.; O'Reilly, E. J.; "Vibrational Spectra and Assignment of Naphthalene and Naphthalene-d-8", *J. Chem. Phys.* 1955, **23**, 238–244. https://doi.org/10.1063/1.1741947
39. Sharaby, Z.; Jagur-Grodzinski, J.; Martan, M.; Vofsi, D.; "Kinetics and mechanism of the anionic polymerization of cyclohexadienes initiated by naphthalene radical anions and dianions", *Journal of Polymer Science: Polymer Chemistry Edition* 1982, **20**, 901–915. https://doi.org/10.1002/pol.1982.170200401
40. Levin, G.; Holloway, B.E.; Szwarc, M.; *J. Am. Chem. Soc.* 1976, 5706–5709.

https://doi.org/10.1021/ja00434a056

41. Melero, C.; Guijarro, A.; Yus, M.; "Structural characterization and bonding properties of lithium naphthaleneradical anion, $[Li^{+}(TMEDA)_2][C_{10}H_8^{\cdot -}]$, and lithium naphthalene dianion $[(Li^{+}TMEDA)_2C_{10}H_8^{-2}]$", *J. Chem. Soc. Dalt. Trans.* 2009, 1286–1289. http://dx.doi.org/10.1039/B821119C
42. Hogen-Esch, T. E.; Smid, J.; "Solvent-Separated Ion Pairs of Carbanions", *J. Am. Chem. Soc.* 1964, **455**, 669–670. https://doi.org/10.1021/ja01081a059
43. Bondarchuk, S. V.; Carrera, M.; Viuda, M. D. L.; Guijarro, A.; "Spontaneous disproportionation of lithium biphenyl in solution: a combined experimental and theoretical study", *New J. Chem.* 2018, **42**, 5168–5177. https://doi.org/10.1039/C7NJ04726F
44. Sodeyama, K.; Yamada, Y.; Aikawa, K.; Yamada, A.; Tateyama, Y.; "Sacrificial Anion Reduction Mechanism for Electrochemical Stability Improvement in Highly Concentrated Li-Salt Electrolyte", *J. Phys. Chem. C* 2014, **118**, 14091–14097. https://doi.org/10.1021/jp501178n
45. Ogata, K.; Salager, E.; Lerr, C. J.; Franser, A. E.; Ducati, C.; Morris, A. J.; Hofman, S.; Grey, C. P.; "Revealing lithium–silicide phase transformations in nano-structured silicon-based lithium ion batteries via in situ NMR spectroscopy", *Nat. Comm.* 2014, **5**, 3217. https://doi.org/10.1038/ncomms4217
46. Woodard, J.C.; Kalisvaart, W.P.; Sayed S. Y.; Olsen, B. C.; Buriak, J. M.; "Beyond Thin Films: Clarifying the Impact of c-$Li_{15}Si_4$ Formation in Thin Film, Nanoparticle, and Porous Si Electrodes", *ACS Appl. Mater. Interfaces.* 2021, **13**, 38147-38160. https://doi.org/10.1021/acsami.1c04293
47. Li, J.; Dahn, J. R.; "An In Situ X-Ray Diffraction Study of the Reaction of Li with Crystalline Si", *J. Electrochem. Soc.* 2007, **154**, A156. https://doi.org/10.1149/1.2409862
48. Usui, H.; Masuda, T.; Sakaguchi, H.; "Li-insertion/extraction Properties of Si Thick-film Anodes in Ionic Liquid Electrolytes Based on Bis(fluorosulfonyl)amide and Bis(trifluoromethanesulfonyl)amide Anions", *Chem. Lett.* 2012, **41**, 521. https://doi.org/10.1246/cl.2012.521